Maximum-Likelihood Estimation for Indicator Dilution Analysis

Maarten P. J. Kuenen*, Ingeborg H. F. Herold, Hendrikus H. M. Korsten, Jean J. M. C. H. de la Rosette, Hessel Wijkstra, and Massimo Mischi, *Senior Member, IEEE*

***Abstract*—Indicator-dilution methods are widely used by many medical imaging techniques and by dye-, lithium-, and thermodilution measurements. The measured indicator dilution curves are typically fitted by a mathematical model to estimate the hemodynamic parameters of interest. This paper presents a new maximum-likelihood algorithm for parameter estimation, where indicator dilution curves are considered as the histogram of underlying transit-time distribution. Apart from a general description of the algorithm, semianalytical solutions are provided for three well-known indicator dilution models. An adaptation of the algorithm is also introduced to cope with indicator recirculation. In simulations as well as in experimental data obtained by dynamic contrast-enhanced ultrasound imaging, the proposed algorithm shows a superior parameter estimation accuracy over nonlinear least-squares regression. The feasibility of the algorithm for use *in vivo* is evaluated using dynamic contrast-enhanced ultrasound recordings obtained with the purpose of prostate cancer detection. The proposed algorithm shows an improved ability (increase in receiver-operating characteristic curve area of up to 0.13) with respect to existing methods to differentiate between healthy tissue and cancer.**

***Index Terms*—Maximum likelihood estimation, physiology, ultrasonography.**

I. Introduction

THE use of indicator- or tracer-dilution methods for hemodynamic quantification in clinical applications has a long history [1]. After injection of an indicator into the bloodstream, an indicator dilution curve (IDC) can be obtained by measurement of the indicator concentration at a desired location downstream as function of time. Hemodynamic parameters of clinical interest can be extracted from IDCs.

Indicator-dilution methods are used in a wide variety of clinical applications. Many techniques were first introduced for cardiovascular quantification, mainly for assessment of cardiac output and blood volumes [1]. The original techniques for IDC measurement, such as dye- and thermodilution, have the drawback of being invasive and requiring patient catheterization [2], [3]. Nowadays, minimally-invasive imaging techniques, such as ultrasound [4], magnetic resonance imaging (MRI) [5], scintigraphy [6], and computed tomography [7], are also available. Their development has led to a wider spectrum of clinical applications, such as detection of ischemia, e.g., in the brain and the myocardium [8], [9]. In other application areas, such as oncology, indicator-dilution methods are used for detection of angiogenesis [5], [10], [11].

The assessment of clinically relevant hemodynamic parameters from IDCs is based on modeling and analysis of the indicator transport kinetics. The first pass of an intravascular indicator can be represented by mathematical models that describe the distribution of indicator transit-times. Apart from providing a stochastic interpretation, several widely adopted models also offer a physiological representation of the hemodynamic phenomena. In fact, the first model proposed by Hamilton *et al.* [3] describes the indicator washout from a single compartment. More recent models, such as the local density random walk (LDRW) model [12], [13], the lognormal model [14]–[16], and the gamma-variate model [17], [18], provide a physiological interpretation for the complete distribution of transit-times.

In many applications, estimation of the hemodynamic parameters of interest is performed by fitting of the IDCs to one of these models. Nonlinear least-squares (NLS) regression is typically adopted for IDC model fitting [19], as it is well known that, in the case of additive white noise, this algorithm provides the maximum-likelihood (ML) estimates for the model parameters. However, IDC noise is not always well described by additive white noise [20]–[22]. As a result, NLS regression may not be the optimal method for IDC parameter estimation.

This paper describes an alternative algorithm based on ML estimation. The stochastic nature of IDC models is exploited by considering the IDC as the observed histogram of indicator transit-times. The statistical properties of this histogram are derived. ML parameter estimation is performed by finding the parameter values that have the highest likelihood of producing

Manuscript received August 7, 2013; revised October 17, 2013; accepted November 3, 2013. Date of publication November 11, 2013; date of current version February 14, 2014. This work was supported by the Dutch Technology Foundation (STW). *Asterisk indicates corresponding author.*

*M. P. J. Kuenen is with the Department of Electrical Engineering, Eindhoven University of Technology, 5612 AZ Eindhoven, The Netherlands and also with the Department of Urology, Academic Medical Center University of Amsterdam, 1105 AZ Amsterdam, The Netherlands (e-mail: m.p.j.kuenen@tue.nl).

I. H. F. Herold and H. H. M. Korsten are with the Department of Electrical Engineering, Eindhoven University of Technology, 5612 AZ Eindhoven, The Netherlands and also with the Department of Anesthesiology, Catharina Hospital, 5623 EJ Eindhoven, The Netherlands (e-mail: ingeborg.herold@catharinaziekenhuis.nl; erik.korsten@catharinaziekenhuis.nl).

J. J. M. C. H. de la Rosette is with the Department of Urology, Academic Medical Center University of Amsterdam, 1105 AZ Amsterdam, The Netherlands (e-mail: j.j.delarosette@amc.uva.nl).

H. Wijkstra is with the Department of Electrical Engineering, Eindhoven University of Technology, 5612 AZ Eindhoven, The Netherlands and also with the with the Department of Urology, Academic Medical Center University of Amsterdam, 1105 AZ Amsterdam, The Netherlands (e-mail: h.wijkstra@amc.uva.nl).

M. Mischi is with the Department of Electrical Engineering, Eindhoven University of Technology, 5612 AZ Eindhoven, The Netherlands (e-mail: m.mischi@tue.nl).

Color versions of one or more of the figures in this paper are available online at http://ieeexplore.ieee.org.

Digital Object Identifier 10.1109/TBME.2013.2290375

the measured transit-time histogram. Apart from a general description of the algorithm, model-specific solutions for the LDRW, lognormal, and gamma-variate models are obtained. In addition, a modification of the algorithm is proposed to cope with the common problem of indicator recirculation.

The performance of the proposed ML algorithm is compared to that of NLS regression in simulations and in IDCs measured *in vitro* by dynamic contrast-enhanced ultrasound (DCE-US) imaging. The feasibility of the algorithm *in vivo* is also shown based on DCE-US data obtained from the prostate microcirculation.

II. Materials and Methods

A. Statistics of Indicator Transit-Time Distributions

An IDC describes the indicator concentration as a function of time at a fixed location downstream, after injection of an indicator bolus upstream. Common models adopted to describe these IDCs, e.g., the LDRW, lognormal, and gamma-variate models, are probability distributions $p(t|\underline{\theta})$ that represent the distribution of indicator transit-times between the injection and the detection sites. The model-specific parameter vector $\underline{\theta}$ defines the IDC shape and, for these three models, offers a direct physiological interpretation of the indicator transport kinetics as well [12], [15], [18].

By interpreting an IDC as a transit-time distribution $p(t|\underline{\theta})$, indicator particles are expected to appear at the detection site at time t with probability $p(t|\underline{\theta})$. The measured transit-time of each indicator particle provides an observation of $p(t|\underline{\theta})$.

In reality, however, the transit-times of individual particles cannot be measured. Ideally, a measured IDC provides the amount of observed indicator particles C at N discrete-time samples n with time step Δt. Hence, the measured IDC $C(n)$ is the observed histogram of $p(t|\underline{\theta})$ based on a total of K transit-time observations. If these observations are independent, the probability that k particles are observed at time n is given by the binomial distribution as

$$P\{C(n)=k\} = \binom{K}{k} p(n\Delta t|\underline{\theta})^k (1-p(n\Delta t|\underline{\theta}))^{K-k}. \quad (1)$$

An example of a simulated IDC based on (1) is shown in Fig. 1. The expectation and the variance of (1) are given as

$$\mathbf{E}\{C(n)\} = Kp(n\Delta t|\underline{\theta}) \quad (2)$$

$$\mathbf{Var}\{C(n)\} = Kp(n\Delta t|\underline{\theta})(1-p(n\Delta t|\underline{\theta})). \quad (3)$$

The expectation $\mathbf{E}\{C(n)\}$ resembles the model IDC; the variance $\mathbf{Var}\{C(n)\}$ represents the fluctuation of the amount of indicator particles and can be considered as noise for the purpose of IDC fitting.

If the transit-time distribution is sampled by a sufficient number of time samples, such that $p(n\Delta t|\underline{\theta}) \ll 1$, the variance approximates the expectation. As a result, the noise power is proportional to the signal amplitude. This relation, which can also be appreciated in Fig. 1, may explain the previously observed correlation between IDC amplitude and IDC noise intensity [20], a correlation that cannot be explained by a standard additive noise model.

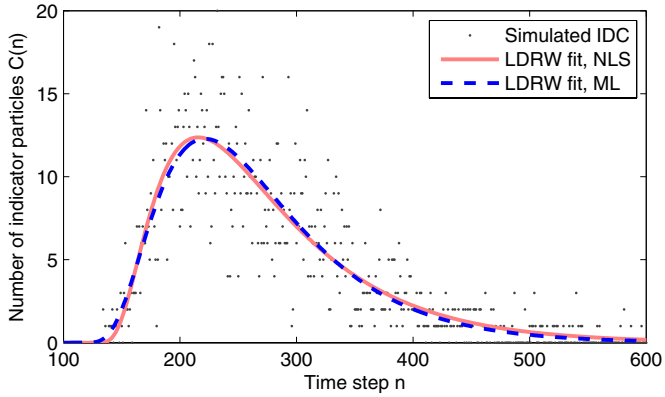

Fig. 1. IDC simulation obtained as histogram of 2000 randomly LDRW-distributed transit-times. The fits based on NLS regression and ML estimation are also shown.

The instantaneous signal-to-noise ratio (SNR) of the IDC is given as

$$\mathrm{SNR}(n) = \frac{(\mathbf{E}\{C(n)\})^2}{\mathbf{Var}\{C(n)\}} = K\frac{p(n\Delta t|\underline{\theta})}{1-p(n\Delta t|\underline{\theta})}. \quad (4)$$

Because the SNR relates linearly to the total number of indicator particles K, K can be used to control the SNR in IDC simulations. The SNR is also influenced by the IDC shape: it is relatively high in narrow IDCs that have relatively high values of $p(n\Delta t|\underline{\theta})$ for only few samples.

B. ML Estimation

Based on the indicator transit-time statistics, we propose an algorithm for ML estimation of the parameter vector $\underline{\theta}$. Given the observed transit-times $t(k)$ of K observed indicator particles, we can evaluate the likelihood $\mathcal{L}(\underline{\theta})$ of the IDC model parameters. If we assume independence of the transit-times of indicator particles, we have

$$\mathcal{L}(\underline{\theta}) = \prod_{k=1}^{K} p(t(k)|\underline{\theta}). \quad (5)$$

The ML solution of the parameters $\underline{\theta}$ is found by maximizing $\mathcal{L}(\underline{\theta})$. In practice, $\ln(\mathcal{L}(\underline{\theta}))$ is often maximized, because the logarithm is a monotonic function that transforms the product into a more simple sum. A logarithmic transformation of (5) yields

$$\ln(\mathcal{L}(\underline{\theta})) = \sum_{k=1}^{K} \ln(p(t(k)|\underline{\theta})). \quad (6)$$

As already discussed, the individual transit-times $t(k)$ are unknown in reality. The transit-time histogram $C(n)$ is obtained instead. We can rewrite (6) in terms of $C(n)$ by grouping all particles that are sampled at the same time sample n as

$$\ln(\mathcal{L}(\underline{\theta})) = \sum_{n=1}^{N} C(n) \ln(p(n\Delta t|\underline{\theta})). \quad (7)$$

In (7), the sum acts on the time samples n rather than on the particles k. The likelihood function (7) equals the correlation between the measured IDC and the logarithm of the adopted IDC model. By differentiation of (7) with respect to $\underline{\theta}$ and equating it to zero, the ML solution for $\underline{\theta}$ can be obtained. This yields

$$\frac{\partial \ln\left(\mathcal{L}(\underline{\theta})\right)}{\partial \underline{\theta}} = \sum_{n=1}^{N} C(n) \frac{\partial p(n\Delta t|\underline{\theta})/\partial \underline{\theta}}{p(n\Delta t|\underline{\theta})} = 0. \quad (8)$$

The obtained result can be used to find the ML estimate $\hat{\underline{\theta}}_{\mathrm{ML}}$ in an iterative numerical optimization scheme. Because $p(n\Delta t|\underline{\theta})$ is a probability distribution that integrates to 1, the area under the IDC (AUC) cannot be included in the preceding analysis. After determination of the IDC shape parameters, AUC can be estimated as the linear scale factor between the measured IDC $C(n)$ and the fit $p(n\Delta t|\hat{\underline{\theta}}_{\mathrm{ML}})$ by, e.g., linear regression.

For three specific IDC models, a partially analytical solution can be derived. As an example, this derivation is provided for the LDRW model in the following section. The derivations for the lognormal and gamma-variate models, which are similar to those for the LDRW model, are reported in the Appendix.

1) Application to the LDRW Model: The LDRW model provides both a stochastic and a physiological interpretation for the transit-time distribution. The model can be derived from a discrete 1-D random walk process [23] and is also an analytical solution of the convective diffusion equation for the 1-D case [12], [24]. The adopted boundary conditions represent a rapid injection and indicator mass conservation. Adopting a modified parameterization $\underline{\theta} = [\mu, \kappa, t_0]$ [25], the distribution of transit-times is given as

$$p(t|\underline{\theta}) = \sqrt{\frac{\kappa}{2\pi(t-t_0)}} \exp\left(-\frac{\kappa\left(t-t_0-\mu\right)^2}{2(t-t_0)}\right). \quad (9)$$

In (9), μ represents the mean transit time (MTT), κ is a skewness parameter related to the dispersion of the indicator bolus through the circulation, and t_0 represents the injection time. The LDRW model has been shown to accurately represent IDCs obtained by DCE-US in different applications, such as for cardiovascular quantification [13], [20] and for analysis of the microcirculation [26]. The model parameter κ has shown a promising value for detection of abnormalities in the microcirculation that are related to cancer [25].

To derive the ML solution for the LDRW model, the model in (9) is differentiated with respect to $\underline{\theta}$ as

$$\frac{\partial p(t|\underline{\theta})}{\partial \mu} = p(t|\underline{\theta}) \cdot \kappa \left(1 - \frac{\mu}{t-t_0}\right) \quad (10a)$$

$$\frac{\partial p(t|\underline{\theta})}{\partial \kappa} = p(t|\underline{\theta}) \cdot \frac{1}{2}\left(\frac{1}{\kappa} - \frac{(t-t_0-\mu)^2}{t-t_0}\right) \quad (10b)$$

$$\frac{\partial p(t|\underline{\theta})}{\partial t_0} = p(t|\underline{\theta}) \cdot \frac{1}{2}\left(\kappa + \frac{1}{t-t_0} - \frac{\kappa\mu^2}{(t-t_0)^2}\right). \quad (10c)$$

We can insert (10) into (8) to obtain the equations that satisfy the ML solution for the LDRW model as

$$\sum_{n=1}^{N}\left(1 - \frac{\mu}{n\Delta t - t_0}\right) C(n) = 0 \quad (11a)$$

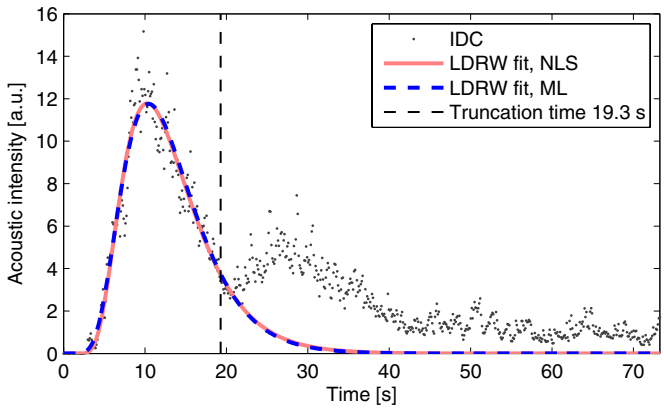

Fig. 2. IDC obtained *in vivo* by DCE-US, in which the tail of the transit-time distribution cannot be observed due to indicator recirculation. Also shown are LDRW model fits based on NLS regression and ML, obtained after truncation of the IDC.

$$\sum_{n=1}^{N}\left(\frac{1}{\kappa} - (n\Delta t - t_0) + 2\mu - \frac{\mu^2}{n\Delta t - t_0}\right) C(n) = 0 \quad (11b)$$

$$\sum_{n=1}^{N}\left(\kappa + \frac{1}{n\Delta t - t_0} - \frac{\kappa\mu^2}{(n\Delta t - t_0)^2}\right) C(n) = 0. \quad (11c)$$

In (11a), we have used the fact that κ is strictly positive. From (11a) and (11b), the ML estimates for μ and κ can be obtained as

$$\hat{\mu}_{\mathrm{ML}} = \frac{\sum_{n=1}^{N} C(n)}{\sum_{n=1}^{N} \frac{C(n)}{n\Delta t - t_0}} \quad (12a)$$

$$\hat{\kappa}_{\mathrm{ML}} = \left[\frac{\sum_{n=1}^{N}(n\Delta t - t_0)C(n)}{\sum_{n=1}^{N} C(n)} - \hat{\mu}_{\mathrm{ML}}\right]^{-1}. \quad (12b)$$

We were not able to find an analytical solution for $\hat{t_{0,\mathrm{ML}}}$. If this parameter is already known, its value can be inserted into (12) to obtain a completely analytical ML solution. If t_0 is unknown, its ML estimate can be obtained by numerically solving (11c) after substitution of κ and μ by their ML solutions given in (12). As a result, the ML parameter estimation problem is significantly less complex than conventional nonlinear regression methods, because iterative optimization is only required for a single parameter.

2) ML and Recirculation: A common issue in IDC analysis is recirculation, i.e., subsequent passages of the indicator bolus that overlap with the tail of the first-pass IDC. As a result, only a limited part of the tail of the transit-time distribution can be observed, as shown in Fig. 2.

Typically, the IDC is truncated by discarding the time segment featuring recirculation from the analysis. Parametric curve-fitting is then applied on the truncated IDC [20]. This approach cannot easily be applied for the proposed ML algorithm, because truncation affects the transit-time distribution that can be observed.

After truncating the IDC at time $t_{\mathrm{Tr}} = n_{\mathrm{Tr}}\Delta t$, the transit-time distribution $p(t|\underline{\theta})$ is no longer completely sampled: transit-times beyond the truncation time t_{Tr} cannot be observed. Instead

of the original distribution, the truncated transit-time distribution is observed. This is given as

$$p_{\mathrm{Tr}}(n\Delta t|\underline{\theta}, n_{\mathrm{Tr}}) = \begin{cases} \dfrac{p(n\Delta t|\underline{\theta})}{\sum_{n=1}^{n_{\mathrm{Tr}}} p(n\Delta t|\underline{\theta})}, & n \leq n_{\mathrm{Tr}} \\ 0, & n > n_{\mathrm{Tr}} \end{cases}. \quad (13)$$

In (13), the scaling term in the denominator ensures that $p_{\mathrm{Tr}}(n\Delta t|\underline{\theta}, n_{\mathrm{Tr}})$ integrates to 1, in order to properly define it as a probability distribution.

The log-likelihood based on the truncated transit-time distribution can be expressed similar to (7) as

$$\ln\left(\mathcal{L}_{\mathrm{Tr}}(\underline{\theta})\right) = \sum_{n=1}^{n_{\mathrm{Tr}}} C(n) \ln\left(p(n\Delta t|\underline{\theta})\right) - \ldots \ln\left(\sum_{n=1}^{n_{\mathrm{Tr}}} p(n\Delta t|\underline{\theta})\right) \sum_{n=1}^{n_{\mathrm{Tr}}} C(n). \quad (14)$$

The derivative of (14) with respect to $\underline{\theta}$ is given as

$$\frac{\partial \ln\left(\mathcal{L}_{\mathrm{Tr}}(\underline{\theta})\right)}{\partial \underline{\theta}} = \left(\sum_{n=1}^{n_{\mathrm{Tr}}} C(n) \frac{\partial p(n\Delta t|\underline{\theta})/\partial \underline{\theta}}{p(n\Delta t|\underline{\theta})}\right) - \ldots \frac{\sum_{n=1}^{n_{\mathrm{Tr}}} \partial p(n\Delta t|\underline{\theta})/\partial \underline{\theta}}{\sum_{n=1}^{n_{\mathrm{Tr}}} p(n\Delta t|\underline{\theta})} \sum_{n=1}^{n_{\mathrm{Tr}}} C(n). \quad (15)$$

The previous semianalytical solutions for the shape parameters, as given in (12a) and (12b), do not represent the ML solution in the case of truncation. For this reason, iterative optimization is adopted to maximize (14). An example IDC model fit obtained by this procedure is shown in Fig. 2. Similar to the original algorithm, the parameter AUC is not included in this analysis, but estimated afterward by linear regression with the fitted IDC.

3) Implementation: All proposed parameter estimation methods were implemented in MATLAB (The Mathworks, Natick, MA, USA), with the routine `mle`. For NLS regression, the routine `lsqcurvefit` was adopted. In both cases, iterative optimization was performed with the built-in trust-region algorithm [27].

In all cases, the parameter t_0 was considered unknown. For all iterative optimization algorithms, parameter initialization was performed as follows. The parameter t_0 was initialized at 2 s before the appearance time, which represents the time at which indicator particles are first observed. The two shape parameters were then initialized using the semianalytical ML algorithm described in Section II-B1 and the Appendix. Finally, AUC was initialized by linear regression as the linear scale factor between the obtained IDC and the initialized IDC.

To prevent numerical issues, a lower bound of 0.5 was adopted for the term $\sum_{n=1}^{n_{\mathrm{Tr}}} p(n\Delta t|\underline{\theta})$ in (14). This lower bound implies that, after truncation, the remaining time samples cover at least half of the original transit-time distribution.

C. Simulation Study

A simulation study was performed to test the proposed ML algorithm. Simulated IDCs were derived as the observed histogram of transit-times, based on random sampling of the transit-time distribution $p(t|\underline{\theta})$ as described in Section II-A. The adopted time step was 0.1 s. An example of a simulated IDC is shown in Fig. 1. Simulations were performed with both $K = 2 \cdot 10^3$ and $K = 5 \cdot 10^3$, which resulted in an SNR of 9 and 13 dB, respectively. These SNR values are in line with those obtained in experimental data.

In this study, simulated IDCs were generated for three models, each using ten different values for the two IDC shape parameters within the following range:

1) LDRW model: $\kappa \in [0.1, 1]$, $\mu \in [10, 40]$.
2) Lognormal model: $\mu \in [2, 3.5]$, $\sigma \in [0.2, 1]$.
3) Gamma-variate model: $\alpha \in [4, 12]$, $\beta \in [1, 4]$.

The parameter range was selected to represent IDCs with MTTs ranging between approximately 10 and 40 s. For each parameter combination, 25 simulated IDCs were obtained. In total, 2500 IDCs were simulated for each model.

All simulated IDCs were fitted by the proposed ML algorithm, as well as by NLS regression. The performance of both parameter estimation methods was evaluated by the bias and standard deviation of the estimated parameters, relative to their true values. This choice was motivated by the wide range of adopted parameter values. In addition, we evaluated the fitting accuracy by the determination coefficient R^2 and the required computation time for all algorithms.

The same IDCs were used to evaluate the parameter estimation performance in case of truncation. The optimal truncation time generally depends on the application. In this study, we adopted a cutoff percentage of 30%, i.e., at t_{Tr}, the model IDC has decayed to 30% of its peak value [23].

In addition, we investigated the variation in the parameter estimates with respect to the cutoff percentage by performing parameter estimation with cutoff percentages ranging between 20% and 40%. The relative standard deviation (expressed as a percentage of the mean) among the parameter estimates obtained with different cutoff percentages was evaluated to measure this variation.

D. Experimental Validation

An experimental validation of the proposed algorithm was performed using DCE-US imaging. An *in vitro* setup was constructed at the Catharina Hospital (Eindhoven, The Netherlands). The setup, which is schematically shown in Fig. 3, consisted of an open network of tubes, in which flow was generated by a centrifugal pump (Medtronic 550 bio-console, Minneapolis, MN, USA). A 0.2 mL SonoVue (Bracco, Milan, Italy) ultrasound-contrast-agent bolus was diluted in 20 mL of saline and subsequently injected into the flow network, which was kept open to avoid recirculation. The hydrostatic pressure was stabilized at the output.

Cross-sectional ultrasound B-mode images were obtained directly before and after the tube network with an iE33 ultrasound imaging system (Philips Healthcare, Andover, MA, USA) and a transesophageal X7-2t probe. Harmonic imaging was applied (2.7–5.4 MHz) at a mechanical index of 0.2. From the obtained image sequences, linearized acoustic time-intensity curves were

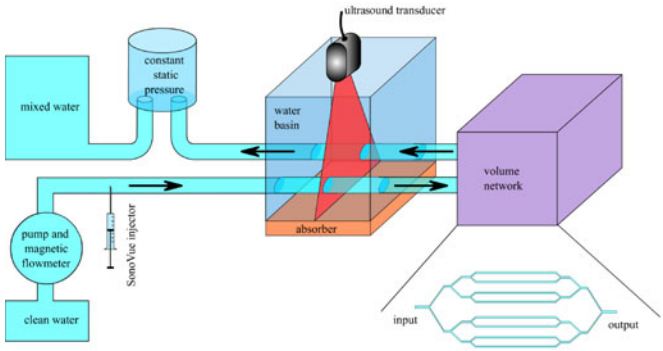

Fig. 3. Schematic overview of the *in vitro* setup.

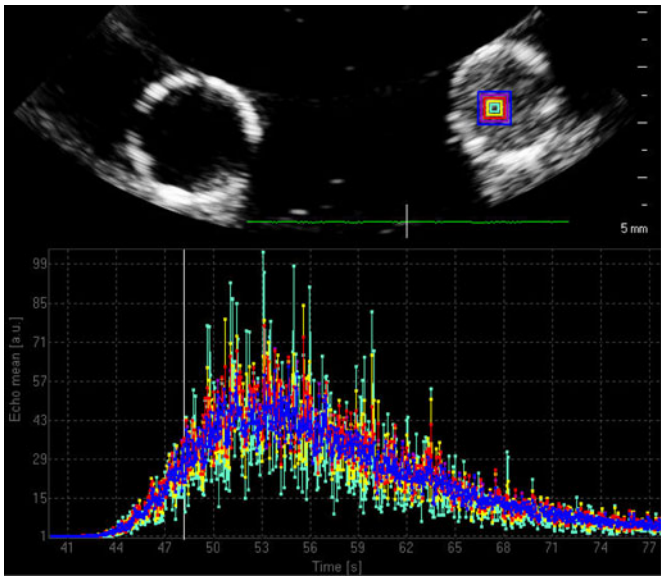

Fig. 4. DCE-US image and acoustic time-intensity curve quantification using QLAB. In the top part, the two tubes for the inflow (left) and outflow (right) of contrast agents are visible. The curves shown in the bottom part are sampled from square ROIs in the top right of the image. The ROI size is indicative of the SNR; the blue IDC, which is least noisy, is sampled from thelargest ROI, whereas the noisy teal IDC is sampled from the smallest ROI.

obtained using QLAB acoustic quantification software (Philips Healthcare, Andover, MA, USA), as shown in Fig. 4.

To avoid the influence of the injection function on our analysis, only the outflow curves were considered in this study. Fig. 4 also shows five square regions of interest (ROIs) of different sizes (from 1.81 to 35.4 mm^2) from which the acoustic time-intensity curves were sampled. The curves in Fig. 4 indicate a correlation between the ROI size and the SNR of the curve. The average SNR, obtained based on the fit with the smallest mean squared error, ranged from 7 dB for the smallest ROI to 14 dB for the largest ROI. Because the number of observed indicator particles K is approximately proportional to the ROI size, this observed correlation between ROI size and SNR can be explained by (4).

For a direct application of indicator dilution theory on the acoustic time-intensity curves, the relation between contrast-agent concentration and measured acoustic intensity must be linear. For low concentrations and low mechanical index, a linear

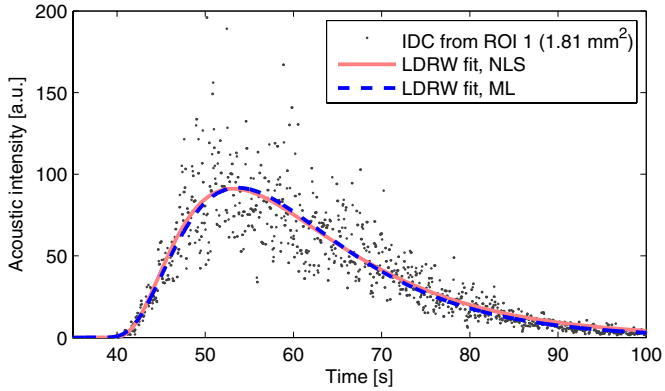

Fig. 5. Experimentally obtained IDC as well as LDRW model fits based on NLS regression and ML.

relation was established by several researchers [20], [25], [28]. As a result, acoustic time-intensity curves may be interpreted directly as IDCs.

Parameter estimation was performed by both ML and NLS using IDCs obtained from 79 experiments, which were performed with four different volumes between 356 and 890 mL and at six different flow values ranging from 1 to 4 L/min. As a result, IDCs were obtained for a wide range of parameter values, as shown in Figs. 4 and 5. In a few curves, the presence of air bubbles resulted in a few noisy samples. To prevent these from affecting the parameter estimation, all IDCs were median filtered with order three prior to curve-fitting.

Because the true values of the parameters were not available, an indirect method was adopted to evaluate the parameter estimation performance. Since the IDCs were sampled from concentric ROIs (see Fig. 4), we expected the associated true parameter values to be constant across the ROIs. Consequently, we considered the variation among the parameter estimates obtained from different ROIs as an indirect error metric. The determination coefficient R^2 was adopted to evaluate the overall quality of curve-fitting. The analysis was performed using the complete IDC for fitting, and also after discarding the IDC tail ($\leq 30\%$ of the peak value). Furthermore, the sensitivity of the estimated parameters with respect to the cutoff percentage was evaluated as described in Section II-C.

E. In Vivo Evaluation

The feasibility of the proposed algorithm for *in vivo* use was evaluated with IDCs obtained by DCE-US imaging of the human prostate with the purpose of cancer detection. Cancer detection has been investigated using various imaging modalities, such as DCE-US and dynamic contrast-enhanced MRI [5], [10], [11], [29], [30], and is based on detection of microvascular changes related to angiogenesis and, therefore, to cancer growth.

This study was performed at the Academic Medical Center University Hospital (Amsterdam, The Netherlands) after approval was granted by the local ethics committee; written informed consent was obtained from all patients prior to this study. 17 DCE-US datasets were obtained from nine patients who underwent radical prostatectomy.

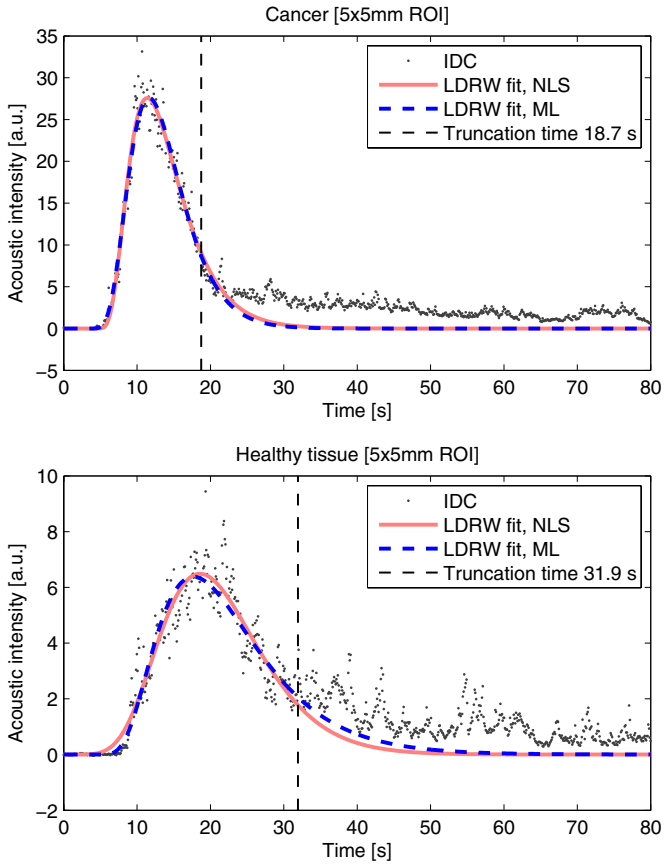

Fig. 6. Top: IDCs obtained *in vivo* from cancer and bottom: healthy tissue. LDRW model fits based on NLS regression and ML are also shown, as well as the truncation time.

Data acquisition was performed using an iU22 ultrasound imaging system (Philips Healthcare, Bothell, WA, USA) and either a C8-4v or C10-3v transrectal probe. The adopted imaging mode was power modulation, at a frequency of 3.5 MHz and a mechanical index of 0.06. In each DCE-US dataset, two IDCs were obtained by QLAB from square ROIs (5 × 5 mm). The ROIs were selected based on the histology ground truth to represent healthy tissue and cancer.

All obtained IDCs were fitted by the LDRW model, using both ML and NLS, as shown in Fig. 6. Because the optimal truncation time is generally difficult to define in these data, all IDCs were fitted using three truncation times, with recirculation cutoff percentages of 30%, 40%, and 50%, respectively. The optimal truncation time was selected based on the minimum mean squared error, averaged between ML and NLS, of the IDC fit. The determination coefficient R^2 was adopted to measure the quality of the obtained IDC fits.

A number of features were extracted from the fitted IDCs in order to evaluate their potential to discriminate between healthy tissue and cancer. We adopted several features that were proposed in the literature [25], [26], [31], namely, the LDRW parameter κ, the parameter AUC, the peak intensity (PI), the full-width at half maximum (FWHM, the period during which the IDC exceeds PI/2), the mean transit time (MTT $= \mu$), and the wash-in time (WIT, the time it takes for the IDC to rise from 5% to 95% of PI).

The tissue classification performance was assessed for each individual parameter using a binary decision threshold. This threshold was shifted over the observed range of parameter values in healthy tissue and cancer. At each threshold level, the sensitivity and specificity for tissue classification were evaluated to derive the receiver-operating characteristic (ROC) curve. The area under the ROC curve was adopted to measure the tissue classification performance [32]. The optimal sensitivity and specificity were determined as the point on the ROC curve closest to ideal classification. A comparison was performed between the parameter estimates obtained by NLS and those obtained by ML.

III. Results

A. Simulation Study

An example of curve-fitting using both NLS and ML is shown in Fig. 1. No significant difference in curve-fitting accuracy was observed between NLS and ML. For $K = 2 \cdot 10^3$, both algorithms fitted the complete IDC with $R^2 = 0.87$ and the truncated IDC (cutoff percentage 30%) with $R^2 = 0.80$. For $K = 5 \cdot 10^3$, these statistics were 0.94 and 0.90, respectively.

The average computation time required to fit one IDC was evaluated on a Windows-based workstation with an Intel Core2Duo processor running at 3.16 GHz with 3.49 GB of RAM. The required computation time for NLS was 0.035 s. For the ML algorithm, the average computation time was 0.032 s for estimation based on the complete IDC, as described in Section II-B1 and the Appendix, and 0.055 s for estimation based on the truncated IDC, as described in Section II-B2.

For each parameter, the estimation accuracy was evaluated by the relative bias and standard deviation with respect to the true values. Table I reports the results for a complete as well as for a truncated IDC fitting. In general, the ML algorithm provided higher estimation accuracy than NLS.

The sensitivity of the parameter estimation with respect to the recirculation cutoff percentage is reported in Table II. For all parameters, ML provided more consistent results than NLS.

B. Experimental Validation

Experimental IDCs were obtained from five ROIs in 79 available recordings. Due to the presence of artifacts in some recordings, we considered only those recordings that could be fitted with an average determination coefficient $R^2 \geq 0.9$ (averaged across all ROIs, both algorithms, and all IDC models). Based on this criterion, the parameter estimation precision by NLS and ML was compared using 71 recordings.

Fitting of the IDCs obtained from these recordings provided an average R^2 (across all models) of 0.94 for ML, compared to 0.95 for NLS. If the IDC was truncated at a recirculation cutoff percentage of 30%, the average R^2 was 0.92 for both algorithms.

The precision of the estimated parameters, assessed as the relative standard deviation among the parameter values estimated

TABLE I
ACCURACY (RELATIVE BIAS ± STANDARD DEVIATION [%]) OF PARAMETER ESTIMATION BASED ON 2500 SIMULATED IDCS PER MODEL

Model & parameter		Estimation based on complete IDC				Estimation based on truncated IDC (cut-off percentage 30%)			
		$K = 2 \cdot 10^3$		$K = 5 \cdot 10^3$		$K = 2 \cdot 10^3$		$K = 5 \cdot 10^3$	
		NLS	ML	NLS	ML	NLS	ML	NLS	ML
LDRW	μ	1.2 ± 13.5	0.0 ± 7.5	0.9 ± 8.5	0.1 ± 4.5	2.7 ± 18.8	0.6 ± 10.6	1.8 ± 12.4	0.2 ± 7.0
	κ	1.5 ± 14.3	0.1 ± 7.7	1.0 ± 9.1	0.2 ± 4.6	3.7 ± 25.8	1.0 ± 17.1	2.4 ± 16.9	0.4 ± 11.4
Lognormal	μ	0.2 ± 2.5	0.0 ± 1.5	0.1 ± 1.6	0.0 ± 1.0	0.5 ± 3.7	0.2 ± 2.6	0.2 ± 2.4	0.0 ± 1.6
	σ	-0.1 ± 7.7	-0.1 ± 4.0	0.0 ± 5.0	0.0 ± 2.5	0.5 ± 13.9	1.5 ± 10.2	0.1 ± 9.2	0.6 ± 6.3
Gamma-variate	α	5.7 ± 28.8	0.6 ± 13.1	2.0 ± 16.5	0.2 ± 7.8	12.7 ± 46.7	0.8 ± 21.4	4.8 ± 25.9	0.2 ± 12.9
	β	0.0 ± 13.9	0.5 ± 7.4	0.1 ± 8.9	0.2 ± 4.5	0.4 ± 21.3	2.3 ± 14.5	0.3 ± 14.2	0.9 ± 9.0

TABLE II
RELATIVE STANDARD DEVIATION [%] AMONG PARAMETER ESTIMATES OBTAINED WITH DIFFERENT RECIRCULATION CUTOFF PERCENTAGES (20%, 25%, 30%, 35%, 40%) IN 2500 SIMULATED IDCS PER MODEL

Model & parameter		$K = 2 \cdot 10^3$		$K = 5 \cdot 10^3$	
		NLS	ML	NLS	ML
LDRW	μ	4.7	2.7	3.1	1.7
	κ	8.2	6.7	5.3	4.3
Lognormal	μ	1.1	0.9	0.7	0.5
	σ	4.6	3.8	3.0	2.3
Gamma-variate	α	12.5	6.5	7.0	3.8
	β	6.5	5.1	4.2	3.1

TABLE III
RELATIVE STANDARD DEVIATION [%] AMONG PARAMETER ESTIMATES OBTAINED FROM VARIOUS ROIS REPRESENTING THE SAME UNDERLYING KINETIC PARAMETERS IN EXPERIMENTALLY MEASURED IDCS FROM 71 RECORDINGS

Model & parameter		Estimation based on complete IDC		Estimation based on truncated IDC (cut-off percentage 30%)	
		NLS	ML	NLS	ML
LDRW	μ	9.0	3.7	7.8	2.9
	κ	9.9	5.0	12.2	6.0
Lognormal	μ	3.7	1.6	3.4	1.3
	σ	8.7	3.7	9.3	4.2
Gamma-variate	α	14.9	6.1	11.0	4.8
	β	7.9	4.0	7.1	3.9

in different ROIs, is reported for all models in Table III, both for fitting the complete IDC and for truncation of the IDC at a recirculation cutoff percentage of 30%. Similar to the simulation results, ML showed a smaller variation in the parameter estimates than NLS for all parameters.

The sensitivity of parameter estimation to the recirculation cutoff percentage is reported for two ROIs in Table IV. For all models, the ML algorithm provided a smaller variation than NLS.

C. *In Vivo Evaluation*

The IDCs obtained *in vivo* were estimated with an average determination coefficient $R^2 = 0.92$ for both algorithms. For several IDC parameters, the classification performance obtained by ML and NLS is reported in Table V. The largest difference in classification performance between ML and NLS was found for κ: the area under the ROC curve obtained by ML was 0.13 larger than that obtained by NLS. For this parameter, the estimates obtained by the two algorithms were compared in a Bland–Altman plot [33], which is shown in Fig. 7. The average difference between κ estimates obtained in cancer and healthy tissue increased by 0.06 if ML was adopted instead of NLS. The parameters AUC and PI showed a very similar classification performance for NLS and ML.

TABLE IV
RELATIVE STANDARD DEVIATION [%] AMONG PARAMETER ESTIMATES OBTAINED WITH DIFFERENT RECIRCULATION CUTOFF PERCENTAGES (20%, 25%, 30%, 35%, 40%) IN EXPERIMENTALLY OBTAINED IDCS FROM 71 RECORDINGS

Model & parameter		ROI 1 (1.8 mm^2)		ROI 5 (35.4 mm^2)	
		NLS	ML	NLS	ML
LDRW	μ	7.3	2.7	6.8	2.8
	κ	16.4	13.4	15.3	12.6
Lognormal	μ	3.1	1.2	3.0	1.1
	σ	12.7	8.0	12.0	7.6
Gamma-variate	α	10.4	4.9	9.3	5.5
	β	8.4	5.4	7.7	5.6

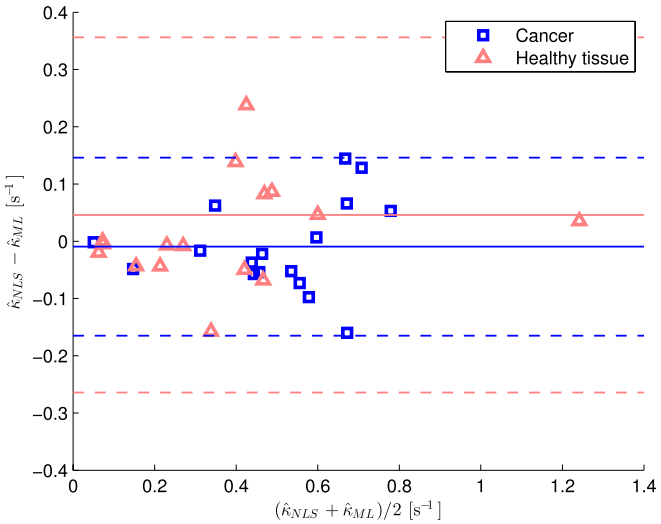

Fig. 7. Bland–Altman plot of the LDRW parameter κ, estimated by both NLS and ML. The solid lines represents the average difference and the dashed lines represent 95% limits of agreement.

TABLE V
SENSITIVITY, SPECIFICITY, AND ROC CURVE AREA FOR TISSUE CLASSIFICATION

Parameter	NLS			ML		
	Sensitivity [%]	Specificity [%]	ROC curve area	Sensitivity [%]	Specificity [%]	ROC curve area
κ	76.5	52.9	0.62	76.5	82.4	0.75
AUC	58.8	82.4	0.69	58.8	82.4	0.70
PI	70.6	70.6	0.73	70.6	70.6	0.73
FWHM	82.4	70.6	0.75	82.4	76.5	0.79
MTT	64.7	64.7	0.64	64.7	64.7	0.62
WIT	52.9	76.5	0.67	52.9	82.4	0.70

IV. DISCUSSION

In all studies, the proposed algorithm provided accurately fitted IDCs. In fact, the obtained determination coefficient R^2, which is theoretically optimized by NLS, was approximately equal for ML and NLS in all studies.

The accuracy of the estimated parameters is, however, more important than the fitting accuracy. To this end, we assessed the bias and standard deviation. Relative statistics were adopted to accommodate for the wide range of parameter values.

The simulation results, reported in Table I, indicate superior results for ML than for NLS for all three adopted models, both with and without truncation. No bias in the parameter estimation was found for either method. The required computation times were similar. Only for fitting of truncated IDCs, the ML algorithm required more computation time than NLS, perhaps because NLS was implemented using a dedicated NLS optimization routine.

In the experimental data, assessment of the parameter estimation accuracy is more complicated, because the true parameter values are unknown. By assuming IDCs sampled from different ROIs (as shown in Fig. 4) to satisfy the same true parameter values, we assessed the precision among parameter estimates obtained from IDCs sampled from different ROIs. Table III shows the parameter estimates obtained by ML to be more consistent across the different ROIs than those obtained by NLS. This result was found for all three adopted models, both with and without IDC truncation.

In applications where indicator recirculation is significant, the definition of the optimal IDC truncation time, minimizing the effect of recirculation on the analysis, is complicated. For this reason, the sensitivity of parameter estimation to the time at which the IDC is truncated was also evaluated. As shown in Table II, the simulation study showed that the ML algorithm is less dependent on the truncation time than NLS. This finding was also confirmed with our experimental data (see Table IV). As a result, ML is more robust with respect to the truncation time choice than NLS.

The *in vivo* evaluation shows the feasibility of the ML algorithm for use in quantitative DCE-US imaging for cancer detection. In fact, for several parameters, the classification ability based on ML is improved with respect to that based on NLS. The classification results of NLS and ML for the IDC amplitude parameters AUC and PI are very similar, probably because the parameter AUC is not included in ML estimation. Because this parameter is estimated afterward by linear regression, the optimization criterium is the same for both algorithms.

For the proposed ML algorithm, IDCs are interpreted as the observed histogram of the transit-time distribution. Although this paper focuses on the first pass of an intravascular indicator, the methodology is applicable for any transit-time distribution. The proposed approach explicitly requires transit-times of indicator particles to be independent. In fact, this assumption follows from the classical assumption in the indicator-dilution theory that the indicator is well mixed with the carrier fluid [34]. Therefore, the independence assumption is merely made explicit by the proposed algorithm.

In general, the log-likelihood function to be maximized, given by (7), equals the correlation between the IDC and the logarithm of the model distribution. With the semianalytical ML solutions, presented for three common indicator dilution models, iterative optimization is not required if the injection time parameter t_0 is known. This may be useful in system identification methods based on two IDCs representing the input and output of the system, where $t_0 = 0$ [13]. In this paper, as often in practice, t_0 was considered unknown. In this case, ML estimation requires iterative optimization for only a single parameter, t_0. The model-specific solutions are valid only if the complete IDC is available for parameter estimation.

Indicator recirculation, a common problem in IDC analysis, is approached by truncation of the transit-time distribution. The modified log-likelihood function, given by (14), contains an additional term that represents the fraction of the AUC that is still observed after truncation.

In the transit-time statistics described in Section II-A, the difference between the observed IDC and its corresponding model curve results from the limited amount of indicator particles K, which represents the sample size of the observed transit-time distribution. As shown in (4), the SNR scales linearly with K. It is particularly low in situations where K is relatively small, e.g., when only a small ROI can be selected to obtain the IDC. This can be observed in Fig. 4.

In a previous study based on DCE-US, it was observed that the IDC noise intensity is correlated with the IDC itself [20]. This correlation can also be observed for the experimental IDCs in Figs. 4 and 5. This phenomenon cannot be explained by standard additive Gaussian noise statistics. It is, however, explained by the modeled transit-time statistics; as formulated in (3), the IDC noise intensity is linearly related to the IDC itself. Because the proposed ML algorithm is based on these statistics, it is

better suited to deal with this phenomenon than standard NLS regression algorithms.

Because measurement inaccuracies are not primarily considered in this paper, the proposed algorithm is generally applicable in a variety of applications. However, if measurement inaccuracies represent the dominant source of errors, the proposed algorithm may not provide optimal results. In this situation, ML estimation should be based on the measurement statistics rather than the transit-time statistics. For example, if the measurement errors are well represented by additive white noise, NLS will provide the most accurate results. For specific acquisition modalities, such as ultrasound and MRI, the statistics of acquisition noise are well documented [21], [22]. In general, the optimal algorithm choice should be based on the measured IDC noise statistics.

In the future, an application-specific parameter estimation method could be developed that optimally deals with both acquisition noise and transit-time statistics. Alternatively, parameter estimation can be optimized with respect to the primary sources of variability.

V. Conclusion

An ML algorithm is presented for the estimation of hemodynamic parameters from IDCs. This algorithm is based on the transit-time statistics of indicator particles. Semianalytical solutions are provided for three commonly adopted IDC models and the algorithm is extended to deal with the typical problem of indicator recirculation. A performance evaluation in simulations as well as in the experimental data obtained by DCE-US shows superior results of the proposed algorithm over NLS regression. In addition, the feasibility of the algorithm is shown with *in vivo* data.

Appendix
ML algorithm for lognormal and gamma-variate models

This appendix reports the ML algorithm for the lognormal and gamma-variate models. Only the main results are provided; the methodology is identical to that described in Section II-B1. Similar to the obtained results for the LDRW model, the solutions provided here are the ML solutions only if the complete IDC is available.

A. Lognormal Model

The lognormal model describes the distribution of indicator transit-times as function of the parameters $\underline{\theta} = [\mu, \sigma, t_0]$ as

$$p(t|\underline{\theta}) = \frac{1}{\sqrt{2\pi}\sigma(t-t_0)} \exp\left(\frac{(\ln(t-t_0)-\mu)^2}{2\sigma^2}\right). \quad (16)$$

The derivative of $p(t|\underline{\theta})$ with respect to $\underline{\theta}$ is given as

$$\frac{\partial p(t|\underline{\theta})}{\partial \mu} = p(t|\underline{\theta}) \cdot \frac{\ln(t-t_0)-\mu}{\sigma^2} \quad (17a)$$

$$\frac{\partial p(t|\underline{\theta})}{\partial \sigma} = p(t|\underline{\theta}) \cdot \frac{\mu^2-\sigma^2-2\mu\ln(t-t_0)+(\ln(t-t_0))^2}{\sigma^3} \quad (17b)$$

$$\frac{\partial p(t|\underline{\theta})}{\partial t_0} = p(t|\underline{\theta}) \cdot \frac{\ln(t-t_0)-\mu+\sigma^2}{\sigma^2(t-t_0)}. \quad (17c)$$

Similar to (12a) and (12b), the ML solution for the shape parameters μ and σ can be written as function of the sampled IDC $C(n)$ and t_0 as

$$\hat{\mu}_{\mathrm{ML}} = \frac{\sum_{n=1}^{N} \ln(n\Delta t - t_0) C(n)}{\sum_{n=1}^{N} C(n)} \quad (18a)$$

$$\hat{\sigma}_{\mathrm{ML}} = \left(\frac{\sum_{n=1}^{N} (\ln(n\Delta t - t_0))^2 C(n)}{\sum_{n=1}^{N} C(n)} - \hat{\mu}_{\mathrm{ML}}^2\right)^{\frac{1}{2}}. \quad (18b)$$

B. Gamma-Variate Model

The indicator transit-time distribution can also be described as a gamma-variate with parameters $\underline{\theta} = [\alpha, \beta, t_0]$ as

$$p(t|\underline{\theta}) = \frac{1}{\beta^\alpha \Gamma(\alpha)} (t-t_0)^{\alpha-1} \exp\left(-\frac{t-t_0}{\beta}\right). \quad (19)$$

The derivative of (19) with respect to $\underline{\theta}$ is

$$\frac{\partial p(t|\underline{\theta})}{\partial \alpha} = p(t|\underline{\theta}) \cdot (\ln(t-t_0) - \ln(\beta) - \psi(\alpha)) \quad (20a)$$

$$\frac{\partial p(t|\underline{\theta})}{\partial \beta} = p(t|\underline{\theta}) \cdot \frac{t-t_0-\alpha\beta}{\beta^2} \quad (20b)$$

$$\frac{\partial p(t|\underline{\theta})}{\partial t_0} = p(t|\underline{\theta}) \cdot \left(\frac{1-\alpha}{t-t_0} + \frac{1}{\beta}\right). \quad (20c)$$

In (20a), $\psi(\alpha) = d(\ln\Gamma(\alpha))/d\alpha$ is the polygamma function of order 1. Similar to the lognormal and LDRW models, the ML solution for the shape parameters α and β can be derived from (20b) and (20c) in semianalytical fashion as

$$\hat{\beta}_{\mathrm{ML}} = \frac{\sum_{n=1}^{N} (n\Delta t - t_0) C(n)}{\sum_{n=1}^{N} C(n)} - \frac{\sum_{n=1}^{N} C(n)}{\sum_{n=1}^{N} \frac{C(n)}{n\Delta t - t_0}} \quad (21a)$$

$$\hat{\alpha}_{\mathrm{ML}} = \frac{\sum_{n=1}^{N} (n\Delta t - t_0) C(n)}{\hat{\beta}_{\mathrm{ML}} \sum_{n=1}^{N} C(n)}. \quad (21b)$$

References

[1] K. Zierler, "Indicator dilution methods for measuring blood flow, volume and other properties of biological systems: A brief history and memoir," *Ann. Biomed. Eng.*, vol. 28, pp. 836–848, 2000.

[2] G. Fegler, "Measurement of cardiac output in anesthetized animals by a thermo-dilution method," *Exp. Physiol.*, vol. 39, no. 3, pp. 153–164, 1954.

[3] W. F. Hamilton, J. W. Moore, J. M. Kinsman, and R. G. Spurling, "Simultaneous determination of the pulmonary and systemic circulation times in man and of a figure related to cardiac output," *Amer. J. Physiol.*, vol. 84, pp. 338–344, 1928.

[4] S. B. Feinstein, B. Coll, D. Staub, D. Adam, A. F. Schinkel, F. J. ten Cate, and K. Thomenius, "Contrast enhanced ultrasound imaging," *J. Nucl. Cardiol.*, vol. 17, no. 1, pp. 106–115, 2010.

[5] P. S. Tofts, "Modeling tracer kinetics in dynamic Gd-DTPA MR imaging," *J. Magn. Reson. Imag.*, vol. 7, no. 1, pp. 91–101, 1997.

[6] H. O. Anger, "Scintillation camera with multichannel collimators," *J. Nucl. Med.*, vol. 5, no. 7, pp. 515–531, 1964.

[7] K. Miles, M. Hayball, A. Dixon, K. Miles, M. Hayball, and A. Dixon, "Colour perfusion imaging: A new application of computed tomography," *Lancet*, vol. 337, no. 8742, pp. 643–645, 1991.

[8] E. Donnemiller, J. Heilmann, G. K. Wenning, W. Berger, C. Decristoforo, R. Moncayo, W. Poewe, and G. Ransmayr, "Brain perfusion scintigraphy with 99mTc-HMPAO or 99mTc-ECD and 123I-beta-CIT single-photon

emission tomography in dementia of the Alzheimer-type and diffuse Lewy body disease," *Eur. J. Nucl. Med.*, vol. 24, no. 3, pp. 320–325, 1997.
[9] K. Wei, A. R. Jayaweera, S. Firoozan, A. Linka, D. M. Skyba, and S. Kaul, "Quantification of myocardial blood flow with ultrasound-induced destruction of microbubbles administered as a constant venous infusion," *Circulation*, vol. 97, pp. 473–483, 1998.
[10] N. Lassau, L. Chami, B. Benatsou, P. Peronneau, and A. Roche, "Dynamic contrast-enhanced ultrasonography (DCE-US) with quantification of tumor perfusion: A new diagnostic tool to evaluate the early effects of antiangiogenic treatment," *Eur. Radiol. Suppl.*, vol. 17, no. 6, pp. F89–F98, 2007.
[11] G. Russo, M. Mischi, W. Scheepens, J. de la Rosette, and H. Wijkstra, "Angiogenesis in prostate cancer: Onset, progression and imaging," *BJU Int.*, vol. 110, pp. E794–E808, 2012.
[12] C. W. Sheppard, *Basic Principles of the Tracer Method*. New York, NY, USA: Wiley, 1962.
[13] M. Mischi, A. A. C. M. Kalker, and H. H. M. Korsten, "Contrast echocardiography for pulmonary blood volume quantification," *IEEE Trans. Ultrason., Ferroelectr., Freq. Control*, vol. 51, no. 9, pp. 1137–1147, Sep. 2004.
[14] R. W. Stow and P. S. Hetzel, "An empirical formula for indicator-dilution curves as obtained in human beings," *J. Appl. Physiol.*, vol. 7, pp. 161–167, 1954.
[15] H. Qian and J. B. Basingthwaighte, "A class of flow bifurcation models with lognormal distribution and fractal dispersion," *J. Theory Biol.*, vol. 205, pp. 161–168, 2000.
[16] M. Mischi, H. C. M. van den Bosch, J. A. den Boer, J. Verwoerd, R. J. E. Grouls, C. H. Peels, and H. H. M. Korsten, "Intra-thoracic blood volume measurement by contrast magnetic resonance imaging," *Magn. Reson. Med.*, vol. 61, pp. 344–353, Jan. 2009.
[17] H. K. Thompson, C. F. Starmer, R. E. Whalen, and H. D. McIntosh, "Indicator transit time considered as a gamma variate," *Circ. Res.*, vol. 14, pp. 502–515, 1964.
[18] M. Mischi, J. A. den Boer, and H. H. M. Korsten, "On the physical and stochastic representation of an indicator dilution curve as a gamma variate," *Physiol. Meas.*, vol. 29, pp. 281–294, 2008.
[19] D. W. Marquardt, "An algorithm for least-squares estimation of nonlinear parameters," *J. Soc. Ind. Appl. Math.*, vol. 11, no. 2, pp. 431–441, 1963.
[20] M. Mischi, A. A. C. M. Kalker, and H. H. M. Korsten, "Videodensitometric methods for cardiac output measurements," *EURASIP J. Appl. Signal Process.*, vol. 5, pp. 479–489, 2003.
[21] R. F. Wagner, S. W. Smith, J. M. Sandrik, and H. Lopez, "Statistics of speckle in ultrasound B-scans," *IEEE Trans. Sonics Ultrason.*, vol. SU-30, no. 3, pp. 156–163, May 1983.
[22] J. Sijbers, A. J. den Dekker, P. Scheunders, and D. van Dyck, "Maximum-likelihood estimation of Rician distribution parameters," *IEEE Trans. Med. Imag.*, vol. 17, no. 3, pp. 357–361, Jun. 1998.
[23] M. Mischi. (2004). "Contrast echocardiography for cardiac quantifications," Ph.D. dissertation, Eindhoven Univ. Technol., [Online]. Available: http://www.sps.ele.tue.nl/members/M.Mischi/
[24] K. H. Norwich and S. Zelin, "The dispersion of indicator in the cardiopulmonary system," *Bull. Math. Biophys.*, vol. 32, pp. 25–43, 1970.
[25] M. P. J. Kuenen, M. Mischi, and H. Wijkstra, "Contrast-ultrasound diffusion imaging for localization of prostate cancer," *IEEE Trans. Med. Imag.*, vol. 30, no. 8, pp. 1493–1502, Aug. 2011.
[26] C. Strouthos, M. Lampaskis, V. Sboros, A. McNeilly, and M. Averkiou, "Indicator dilution models for the quantification of microvascular blood flow with bolus administration of ultrasound contrast agents," *IEEE Trans. Ultrason., Ferroelectr., Freq. Control*, vol. 57, no. 6, pp. 1296–1310, Jun. 2010.
[27] R. H. Byrd, J. C. Gilbert, and J. Nocedal, "A trust region method based on interior point techniques for nonlinear programming," *Math. Prog.*, vol. 89, no. 1, pp. 149–185, 2000.
[28] M. Lampaskis and M. Averkiou, "Investigation of the relationship of nonlinear backscattered ultrasound intensity with microbubble concentration at low MI," *Ultrasound Med. Biol.*, vol. 36, no. 2, pp. 306–312, 2010.
[29] M. Smeenge, J. J. M. C. H. de la Rosette, and H. Wijkstra, "Current status of transrectal ultrasound techniques in prostate cancer," *Curr. Opin. Urol.*, vol. 22, pp. 297–302, 2012.
[30] M. P. J. Kuenen, T. A. Saidov, H. Wijkstra, and M. Mischi, "Contrast-ultrasound dispersion imaging for prostate cancer localization by improved spatiotemporal similarity analysis," *Ultrasound Med. Biol.*, vol. 39, no. 9, pp. 1631–1641, 2013.
[31] N. Elie, A. Kaliski, P. Péronneau, P. Opolon, A. Roche, and N. Lassau, "Methodology for quantifying interactions between perfusion evaluated by DCE-US and hypoxia throughout tumor growth," *Ultrasound Med. Biol.*, vol. 33, no. 4, pp. 549–560, 2007.
[32] M. H. Zweig and G. Campbell, "Receiver-operating characteristic (ROC) plots: A fundamental evaluation tool in clinical medicine," *Clin. Chem.*, vol. 39, pp. 561–577, 1993.
[33] J. M. Bland and D. G. Altman, "Statistical methods for assessing agreement between two methods of clinical measurement," *Lancet*, vol. 327, no. 8476, pp. 307–310, 1986.
[34] K. L. Zierler, "Theoretical basis of indicator-dilution methods for measuring flow and volume," *Circ. Res.*, vol. 10, pp. 393–407, 1962.

Maarten P. J. Kuenen received the M.Sc. degree in electrical engineering from the Eindhoven University of Technology, Eindhoven, The Netherlands, in 2009. After receiving his M.Sc. degree, he was researcher at the Academic Medical Center, University of Amsterdam, The Netherlands, where he contributed to the development of accurate validation techniques for prostate cancer imaging methods.

Since 2009, he has been working towards a Ph.D. degree at the Eindhoven University of Technology, in close collaboration with the Academic Medical Center, University of Amsterdam, the Netherlands. His research focuses on the development of quantitative contrast-enhanced ultrasound imaging techniques for localization of prostate cancer.

Ingeborg H. F. Herold was born in Utrecht, The Netherlands, in 1970. She graduated in medicine at the University of Leuven, Leuven, Belgium, in 1998.

She was a Resident in Anesthesiology at the Erasmus University Medical Center, Rotterdam, The Netherlands and followed a fellowship in Intensive Care at the Leiden University Medical Center, Leiden, The Netherlands. After her traineeship, she was a Staff Member for more than two years in Intensive-care at the University Medical Center Utrecht, Utrecht, The Netherlands. Since 2008, she has been working at the Catharina Hospital, Eindhoven, The Netherlands, as an Anesthesiologist-Intensivist. In collaboration with the Eindhoven University of Technology, Eindhoven, The Netherlands, she is involved in a research project for the Ph.D. degree on intrathoracic blood volume measurement with contrast enhanced ultrasound.

Hendrikus H. M. Korsten graduated in medicine from the University of Groningen, Groningen, The Netherlands, in 1978. During his training as an Anesthesiologist at the University of Utrecht, Utrecht, The Netherlands, he started the Ph.D. study on the measurement of intrathoracic fluid content during open-heart surgery, for which he received the Ph.D. degree form the University of Leiden, Leiden, The Netherlands, in 1984.

Since June 1983, he has been a Staff Member in the Department of Anesthesiology, Intensive Care, and Pain-Treatments, Catharina Hospital, Eindhoven, The Netherlands. From 1989 until 1993, he was the Chairman of the professional medical staff of this hospital. He is also an Intensivist and was the Head of the Intensive Care during 1993–2001. He was one of the initiators of a national intensive-care database. He was also involved in research projects on data storage and data mining of patient data, as well as the development of artificial intelligence in the intensive care. Since 2001, he has been a Part-time Professor at the Eindhoven University of Technology, Eindhoven, The Netherlands.

Jean J. M. C. H. de la Rosette graduated in medicine from the Radboud University Hospital, Nijmegen, The Netherlands, in 1992. In 1993, he obtained his Doctorate degree from the same University.

In 1992, he was appointed as a Consultant Urologist and the Director Minimal Invasive Urology in the Department of Urology at the Radboud University Hospital. Since 2002, he has been a Professor and Chairman of the Department of Urology, Academic Medical Center, University of Amsterdam, Amsterdam, The Netherlands. He has published more than 300 peer-reviewed articles in the field of urology with special focus on minimally invasive therapy, oncological urology, and endourology.

Prof. de la Rosette is a member of various urological societies including the American Urological Association, the European Association of Urology, the Endourological Society, and the Société International d'Urologie.

Hessel Wijkstra received the M.Sc. degree in electrical engineering, and the Ph.D. degree from both from the Twente University of Technology, Enschede, The Netherlands, with the Ph.D. thesis "The flow pulse response of the ventricular pressure source."

He has been performing biomedical research in the Department of Urology of the Radboud University Hospital, Nijmegen, The Netherlands. Since 2004, he has been a Faculty Member in the Department of Urology, Academic Medical Center, University of Amsterdam, Amsterdam, The Netherlands. Since November 2010, he has been a Part-time Professor at the Eindhoven University of Technology, Eindhoven, The Netherlands, focusing on the clinical validation and implementation of contrast-enhanced ultrasound techniques. His main research interest includes imaging, particularly contrast-enhanced ultrasound, in the diagnosis and treatment of prostate and kidney cancer.

Massimo Mischi (SM'10) received the M.Sc. degree in electrical engineering from La Sapienza University, Rome, Italy, in 1999, and the Ph.D. degree from the Eindhoven University of Technology, Eindhoven, The Netherlands, in 2004.

In 2007, he became an Assistant Professor, and since 2011, he has been an Associate Professor in the Department of Electrical Engineering at the Eindhoven University of Technology, where he coordinates the Biomedical Diagnostics Research Team. His research interests include model-based quantitative analysis of biomedical signals, with focus on ultrasound and magnetic resonance imaging, and on electrophysiology.

Dr. Mischi received the Dutch VIDI Grant in 2009 and the European ERC Starting Grant in 2011 for his research on angiogenesis imaging by contrast-enhanced ultrasound. He is the Vice-chairman of the IEEE Engineering in Medicine and Biology Society Benelux Chapter and the Secretary of the Dutch Society of Medical Ultrasound.